Structure of Shroom domain 2 reveals a three-segmented coiled-coil required for dimerization, Rock binding, and apical constriction

Swarna Mohan[a], Ryan Rizaldy[a], Debamitra Das[a], Robert J. Bauer[b], Annie Heroux[c], Michael A. Trakselis[b], Jeffrey D. Hildebrand[a], and Andrew P. VanDemark[a]

[a]Department of Biological Sciences and [b]Department of Chemistry, University of Pittsburgh, Pittsburgh, PA 15260; [c]Department of Biology, Brookhaven National Laboratory, Upton, NY 11973

ABSTRACT **Shroom (Shrm) proteins are essential regulators of cell shape and tissue morphology during animal development that function by interacting directly with the coiled-coil region of Rho kinase (Rock). The Shrm–Rock interaction is sufficient to direct Rock subcellular localization and the subsequent assembly of contractile actomyosin networks in defined subcellular locales. However, it is unclear how the Shrm–Rock interaction is regulated at the molecular level. To begin investigating this issue, we present the structure of Shrm domain 2 (SD2), which mediates the interaction with Rock and is required for Shrm function. SD2 is a unique three-segmented dimer with internal symmetry, and we identify conserved residues on the surface and within the dimerization interface that are required for the Rock–Shrm interaction and Shrm activity in vivo. We further show that these residues are critical in both vertebrate and invertebrate Shroom proteins, indicating that the Shrm–Rock signaling module has been functionally and molecularly conserved. The structure and biochemical analysis of Shrm SD2 indicate that it is distinct from other Rock activators such as RhoA and establishes a new paradigm for the Rock-mediated assembly of contractile actomyosin networks.**

Monitoring Editor
Benjamin Margolis
University of Michigan
Medical School

Received: Nov 22, 2011
Revised: Feb 23, 2012
Accepted: Mar 29, 2012

INTRODUCTION

Members of the Shroom (Shrm) family of cytoskeletal adaptor proteins bind to Rho-associated coiled-coil kinase (Rock) and are important determinants of cytoskeletal organization, cellular behavior, and tissue shape (Hildebrand and Soriano, 1999; Fairbank *et al.*, 2006; Hagens *et al.*, 2006b; Nishimura and Takeichi, 2008; Taylor *et al.*, 2008; Lee *et al.*, 2009; Chung *et al.*, 2010; Plageman *et al.*, 2010). In vertebrates, the Shrm family consists of four members, Shrm1–4 (Hagens *et al.*, 2006a), and many of these have been implicated in the morphogenesis of cells and tissues, including the neural tube (Hildebrand and Soriano, 1999), the eye (Lee *et al.*, 2009; Plageman *et al.*, 2010), vasculature (Farber *et al.*, 2011), neurons (Taylor *et al.*, 2008), and intestines (Chung *et al.*, 2010; Plageman *et al.*, 2011). Shrm family members have also been implicated in X-linked mental retardation (Hagens *et al.*, 2006b) and renal function (Kottgen *et al.*, 2009) in humans. All Shrm proteins tested control cell morphology and tissue architecture by regulating the subcellular distribution of actomyosin networks and use these to elicit apical constriction or cortical contractility (Hildebrand, 2005). Shrm proteins are also found in most invertebrates, and analysis of *Drosophila* Shrm (dShrm) suggests that the principal functions of these proteins are conserved

This article was published online ahead of print in MBoC in Press (http://www.molbiolcell.org/cgi/doi/10.1091/mbc.E11-11-0937) on April 4, 2012.

S.M., J.D.H., and A.P.V. conceived and designed the study. S.M. carried out all aspects of crystallization and structure determination, except data collection at the National Synchrotron Light Source at Brookhaven National Laboratory, which was performed by A.H. R.R. and S.M. performed the biochemical analyses. D.D. performed the cell-based apical constriction assays. R.J.B. and M.A.T. performed and analyzed the fluorescence energy transfer assays. A.P.V. and J.D.H. wrote the manuscript with input from S.M. and M.A.T.

The authors declare that they have no conflict of interest.

Address correspondence to: Andrew P. VanDemark (andyv@pitt.edu), Jeffrey D. Hildebrand (jeffh@pitt.edu).

Abbreviations used: HD, homodimerization; SBD, Shroom-binding domain; SC, surface cluster; SD2, Shroom domain 2; Shrm, Shroom.

(Dietz *et al.*, 2006; Bolinger *et al.*, 2010). The activity of all Shrm proteins is contingent upon proper subcellular localization and their ability to bind Rock (Haigo *et al.*, 2003; Hildebrand, 2005; Plageman *et al.*, 2010). The Shrm–Rock interaction is mediated by the highly conserved Shrm domain 2 (SD2), located at the C-termini of all Shrm proteins (Hildebrand, 2005; Dietz *et al.*, 2006).

Myosin II and the actin cytoskeleton are universally used by cells to control shape and behavior in response to environmental stimuli during a wide range of biological processes. The activity of myosin II is tightly controlled through phosphorylation of the associated myosin regulatory light chains by a number of serine/threonine kinases and phosphatases (Ikebe *et al.*, 1988; Moussavi *et al.*, 1993). One of these kinases is Rock (Amano *et al.*, 1996a; Ishizaki *et al.*, 1996), which has been shown to regulate myosin II activity directly by phosphorylating Ser-19 of the myosin light chain and indirectly by inhibiting the activity of the myosin phosphatase (Amano *et al.*, 1996a; Kimura *et al.*, 1996; Kawano *et al.*, 1999). The activity of Rock appears to be tightly controlled via several mechanisms. Primary among these is relief of intramolecular inhibition of the kinase domain by its C-terminus. This is typically achieved by the binding of GTP-bound RhoA to the Rho-binding domain located within the coiled-coil region of Rock (Ishizaki *et al.*, 1996; Matsui *et al.*, 1996). It is predicted that RhoA binding causes a conformation change within Rock that displaces the C-terminus from the kinase domain and allows for catalytic activity (Amano *et al.*, 1996b, 1999). SD2 of Shrm has also been shown to interact with the coiled-coil region of Rock but at a location that is distinct from the Rho-binding domain (Nishimura and Takeichi, 2008; Taylor *et al.*, 2008; Bolinger *et al.*, 2010; Farber *et al.*, 2011).

Although structures have been determined for many portions of Rock, including the kinase domain (Jacobs *et al.*, 2006; Yamaguchi *et al.*, 2006a, 2006b; Komander *et al.*, 2008), PH domain (Wen *et al.*, 2008), portions of the coiled-coil domain (Shimizu *et al.*, 2003; Tu *et al.*, 2011), and a RhoA:Rho-binding domain complex (Dvorsky *et al.*, 2004), there is no structural information on the Shrm-binding domain of Rock and no structural information for any portion of Shrm. Consequently, there is little information regarding the molecular details of the Shrm–Rock interaction or how Shrm binding affects the activation status of Rock. Here, we take a structural approach to gain molecular and mechanistic insight into SD2 of Shrm and its interaction with Rock.

RESULTS

SD2 adopts an extended three-segmented coiled-coil

To understand the molecular basis for Shrm-mediated regulation of actomyosin contractility, we initiated a structural analysis of Shrm proteins. These studies focused on the C-terminal SD2 since it is the most highly conserved domain found in all Shrm family members and is both necessary and sufficient for activating actomyosin contractility (Hildebrand, 2005). Limited proteolysis of various SD2-containing protein fragments derived from mouse Shrm3 indicates the presence of a stable "core" of ~180 residues located at the C-terminus of SD2. We used these data to guide the design of SD2 expression constructs from several different Shrm proteins. We were able to obtain and optimize crystals from dShrm containing amino acid residues 1393–1576 (Figure 1A) and determine its structure using the SAD method with selenomethionine (SeMET)-substituted crystals (see *Material and Methods* and Table 1 for a complete description of the structure determination procedure).

The structure is refined at 2.7-Å resolution with an R_{free} value of 27.4%. The asymmetric unit contains a complete SD2 dimer, with only minor disorder observed at the termini of each chain. The SD2 dimer adopts a highly unusual fold consisting of three antiparallel coiled-coil segments (Figure 1B). Each monomer contains three helices, with the B helix being roughly twice the length of the A and C helices. The B helices wrap around each other to form a "body" segment of 85 residues, whereas the A and C helices pair to form ~45-residue "arm" segments (Figure 1B and Supplemental Figure S1). Within both the arm and body segments, coiled-coil interactions establish an extensive dimer interface, burying 4577 Å^2 of surface area. This interface contains many conserved leucine and isoleucine residues, making interactions within the dimer interface reminiscent of leucine-zipper domains. In contrast to Shrm SD2, leucine zippers are most often parallel dimers; however, we note that the structural database contains a large and diverse collection of coiled-coil–containing proteins in both parallel and antiparallel arrangements. To confirm that SD2 forms a dimer in solution, we

	SeMET (SAD)	Native
Data collection		
Space group	$P2_12_12$	$P2_12_12$
Cell dimensions		
a (Å)	72.2	72.8
b (Å)	84.9	85.6
c (Å)	93.0	93.0
Resolution (Å)	30.0–3.5 (3.56–3.50)	50.0–2.7 (2.75–2.70)
Unique reflections	7573	16,446
R_{merge}	8.5 (8.2)	6.9 (46.3)
I/σI	42.1 (34.1)	34.2 (3.5)
Completeness (%)	99.3 (100)	99.9 (99.9)
Redundancy	10.0 (10.7)	8.5 (8.1)
Refinement		
Resolution (Å)		47.0–2.7
R_{work}/R_{free}		22.78/28.38
Number of protein atoms		2749
Root mean square deviations		
Bond lengths (Å)		0.10
Bond angles (deg)		0.600
Average isotropic B values (Å^2)		75.9
Ramachandran statistics		
Outliers		0
Allowed		0
Favored		100

Values in parentheses correspond to those in the outer resolution shell.
$R_{merge} = (|(\Sigma I - \langle I \rangle)|)/(\Sigma I)$, where <I> is the average intensity of multiple measurements.
$R_{work} = \Sigma_{hkl} \, ||F_{obs}(hkl)|| - F_{calc}(hkl)||/\Sigma_{hkl} \, |F_{obs}(hkl)|$.
R_{free} = cross-validation R factor for 7.3% of the reflections against which the model was not refined.

TABLE 1: Data collection and refinement statistics for dShrm SD2.

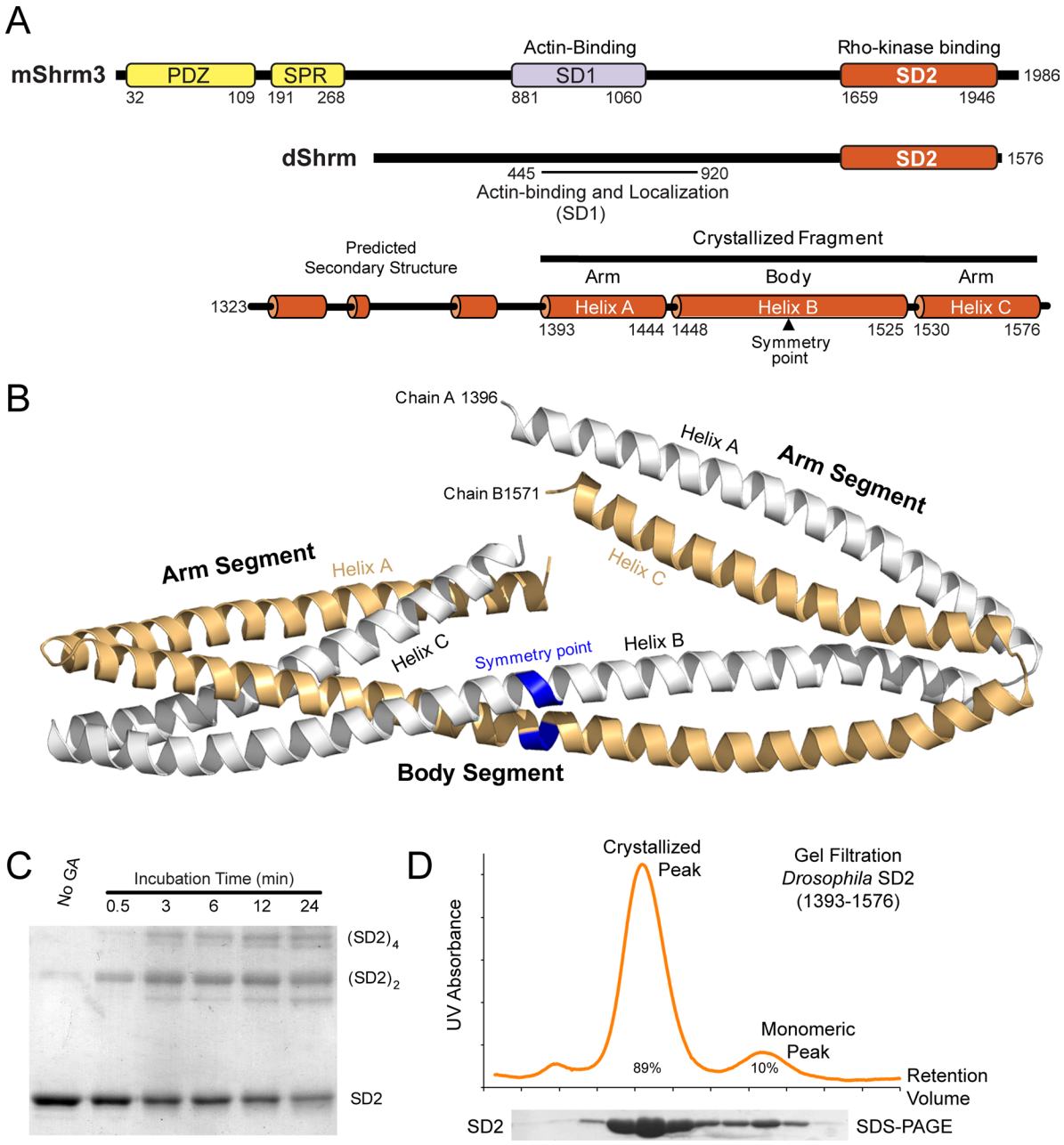

FIGURE 1: Structure of the dShrm SD2 dimer. (A) Domain organization for the Shroom proteins used in this study. The predicted secondary structure for the canonical SD2 and the actual secondary structure and the location of relevant features from the crystallized fragment are shown. (B) Ribbon diagram of the dShrm SD2 dimer. The body segment, two arm segments, and the symmetry point locations are indicated. (C) Chemical cross-linking of dShrm SD2. Purified dShrm SD2 was incubated with 0.009% glutaraldehyde over the indicated time period and the resulting species separated by SDS–PAGE. (D) Gel filtration profile of wild-type dShrm SD2. Two species are observed, and the relative peak area from each is indicated. Fractions collected during this run were analyzed by SDS–PAGE and indicated below the trace.

treated purified SD2 with the chemical cross-linker glutaraldehyde and resolved the resulting species on SDS–PAGE (Figure 1C). These assays indicate that we can readily detect a dimeric SD2 species in solution (Figure 1C). In fact in the absence of cross-linker, a small dimeric fraction is still observed in the SDS–PAGE gel, indicating the strength of interaction in the coiled-coil. In this assay, we can also detect tetrameric and other higher-order species that appear to be formed by spurious cross-linking between SD2 dimers. Because this technique is not quantitative (Trakselis *et al.*, 2005), we further characterized SD2's solution state using gel filtration (Figure 1D). We observe two species in this assay: a larger dimeric species that was used for crystallization and a minor peak containing 9% of the peak area. These data indicate that the dimeric species we observe in the crystal is the predominant species in solution.

There are notable regions of both symmetry and asymmetry within SD2. The molecule is internally symmetric, with the left and right half-dimers exhibiting near structural identity (root mean square deviation of 0.6 Å over 174 Cα atoms; Figure 1B and Supplemental

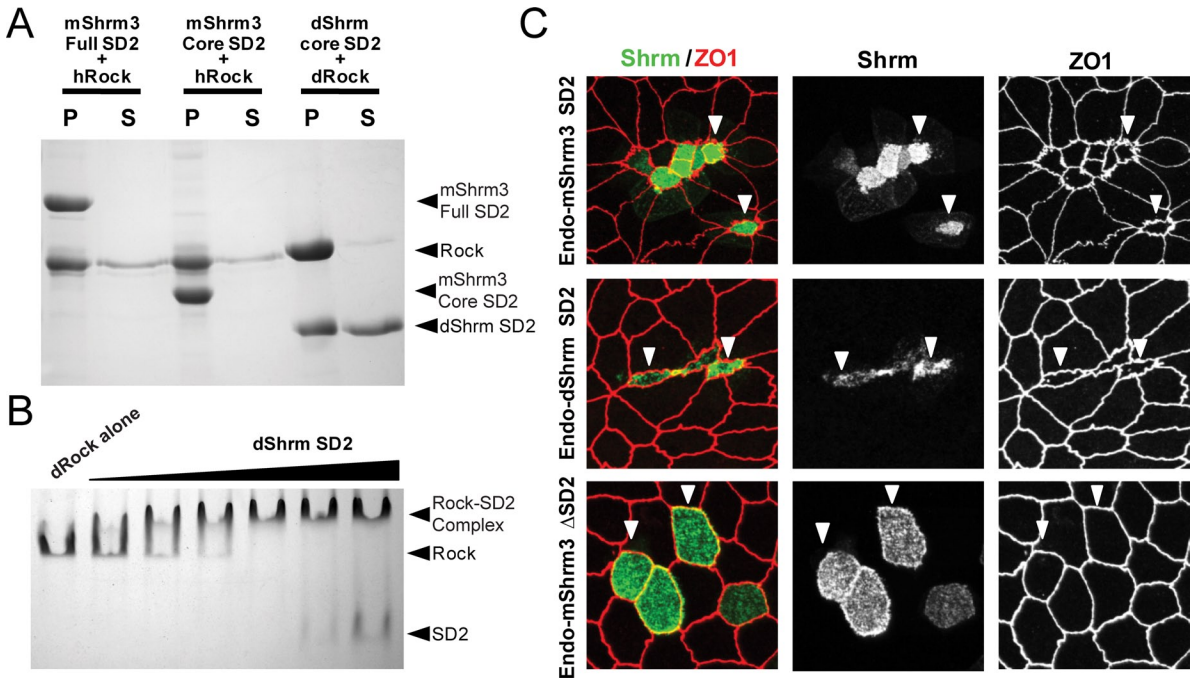

FIGURE 2: The SD2 core is sufficient for Rock binding and apical constriction. (A) Purified His-tagged mShrm3 full SD2 (1643–1986), His-tagged mShrm3 SD2 core (1762–1952), or His-tagged dShrm SD2 core (1393–1576) was mixed with either hRock (707–938) or dRock (724–948) as indicated and complexes detected by pull-down with Ni beads. P, pellet fraction; S, supernatant fraction. (B) Native-PAGE of dShrm SD2 alone and mixed with increasing concentrations of dShrm SD2. Complex formation is monitored by the formation of a slower-migrating species. (C) Endolyn-tagged Shrm constructs were expressed in MDCK cells, and cells were stained to detect the exogenous endolyn–Shrm protein (green) and ZO-1, a marker for tight junctions (red). Both mShrm3 SD2 and dShrm SD2 can cause apical constriction upon being targeted to the apical membrane. Arrowheads denote cells expressing endolyn–Shrm proteins.

Figure S2). We term the point separating the left and right halves of the dimer the symmetry point. Of interest, there is a twist within the dimer such that the right and left arms are rotated ~60° relative to the long axis of the body segment, which introduces an element of asymmetry into the overall structure (Figure 1B and Supplemental Figure S2). Structural homology searches failed to identify any structures whose similarity with Shrm extends beyond a single coiled-coil segment, indicating that the structure we observe may be unique. More important, the structure of SD2 is distinct from that of RhoA, the other known activator of Rock that binds to the coiled-coil region.

The dShrm SD2 core is sufficient for dRock binding and apical constriction

Previous studies showed that the direct interaction between SD2 of mouse Shrm3 (1563–1986) and the coiled-coil domain of human Rock (698–957) is required for apical constriction (Nishimura and Takeichi, 2008). In addition, we also showed that this interaction is conserved in dShrm and dRock (Bolinger *et al.*, 2010). Our structure is missing the N-terminal 70 residues of the previously defined SD2 (Dietz *et al.*, 2006), as these were removed to facilitate crystallization. To demonstrate that the structure we observed still contained the biologically relevant portion of the SD2, we examined the ability of SD2 regions from mShrm3 and dShrm to both interact with Rock and mediate apical constriction in a cell-based assay. To examine the Shrm–Rock interaction, we first performed pull-down assays using histidine (His)-tagged Shrm-SD2 constructs containing the core fragment from dShrm, the equivalent core fragment from mouse Shrm3 (1762–1952), or a longer form of mouse Shrm3 (1543–1985), which is similar in length to the SD2s that are shown to cause apical constriction (Hildebrand, 2005; Dietz *et al.*, 2006; Figure 2A). For Rock, we used amino acids 707–946 of human Rock1 and amino acids 724–938 of *Drosophila* Rock. These sequences were chosen based on the previously described Shrm-binding sequences (Nishimura and Takeichi, 2008; Bolinger *et al.*, 2010; Farber *et al.*, 2011), sequence conservation, and predicted secondary structure. We refer to these regions of hRock and dRock as the Shrm-binding domain (SBD). Because this sequence is 95% identical between mouse and human Rock, we predicted that human Rock should bind equally well to mouse Shrm3. In this assay, all three SD2 fragments are able to bind Rock, indicating that the crystallized fragment of dShrm contains a Rock-binding surface and that this surface is likely conserved in all SD2s. To follow up on these findings, we tested by native gel electrophoresis whether Rock and Shrm could form a stable complex (Figure 2B). Results indicate that the Shrm–Rock interaction is stable, saturable, and stoichiometric. Finally, to demonstrate that the SD2 regions of mShrm3 and dShrm exhibit equivalent functions in vivo, we tested their ability to mediate apical constriction in cultured Madin–Darby canine kidney (MDCK) cells. The C-terminal regions of dShrm (residues 1144–1576) and mShrm3 (residues 1372–1976), containing the SD2 motifs, were expressed as chimeric fusion proteins consisting of the apically targeted transmembrane protein endolyn (Hildebrand, 2005). We also expressed a fusion protein containing mShrm3 1372–1562 (lacking the SD2) as a negative control. MDCK cells transiently transfected with these expression vectors were grown on Transwell filters and stained to detect the tight-junction marker ZO1 and the ectopically expressed endolyn–Shrm protein. The distribution of ZO-1 (red) indicates the

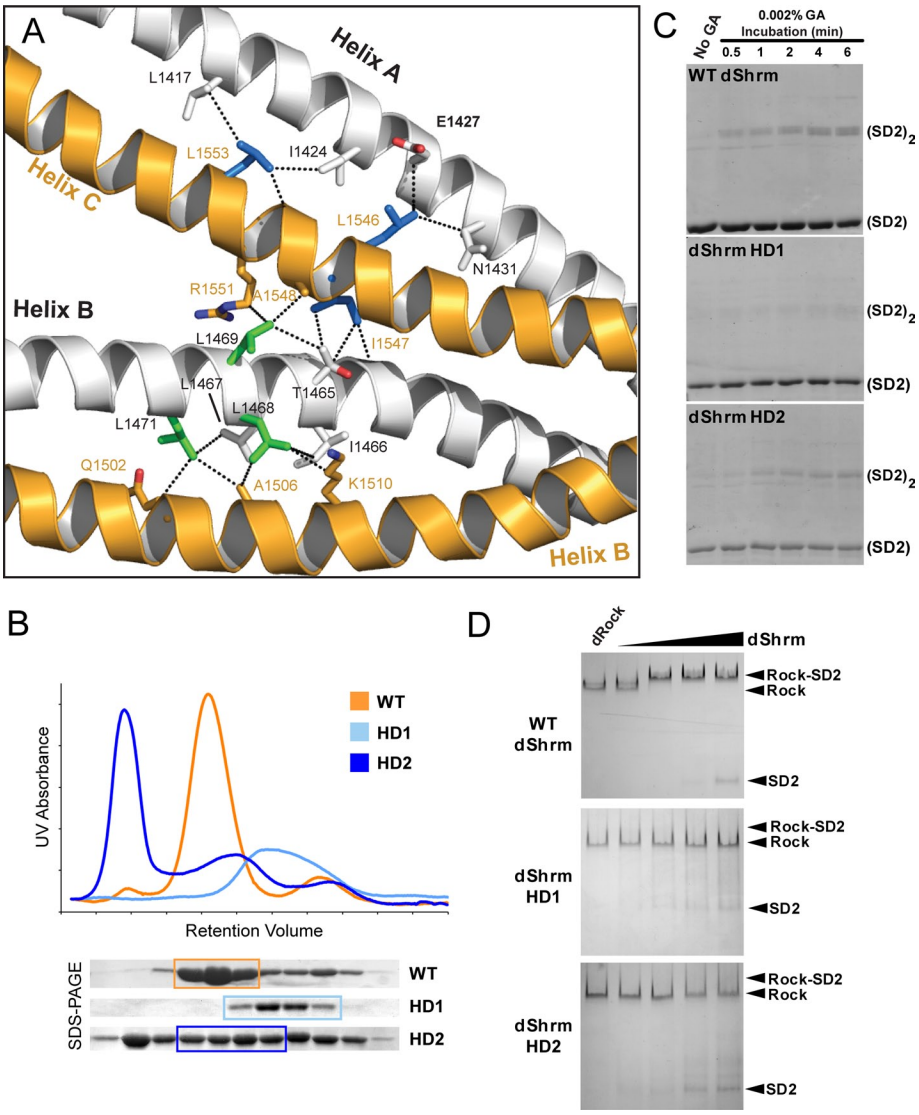

FIGURE 3: Mutations in the dimerization interface diminish Rock binding. (A) Ribbon diagram of SD2 highlighting the interface mutations, HD1 (green), and HD2 (blue). Residues making contacts with HD1 or HD2 are shown as white (chain A) or gold (chain B) sticks. (B) Gel filtration chromatograms for wild-type and HD1 and HD2 mutant proteins. SDS–PAGE of resulting fractions aligned to the chromatogram is shown below. (C) Chemical cross-linking of wild-type and HD1 and HD2 mutant proteins. The indicated dShrm SD2 protein was incubated with 0.002% glutaraldehyde. Samples were taken at the indicated time points and resolved by SDS–PAGE. (D) Native gel electrophoresis of dRock 724–938 mixed with increasing concentrations of wild-type and HD mutant dShrm–SD2 proteins.

apical boundaries, whereas Shrm (green) localization indicates that all three fusions were expressed and targeted to the apical plasma membrane. Cells expressing an endolyn fusion containing an intact SD2 are able to constrict, whereas the control endolyn–Shrm3 fusion is unable to perform apical constriction (Figure 2C). Therefore we conclude that the crystallized SD2 contains the Rock-binding site and, when properly localized, is sufficient to mediate apical constriction.

Perturbation of the SD2 dimerization interface inhibits Rock binding

We next examined whether the SD2 dimerization interface was important for Rock binding, reasoning that the extended shape observed for SD2 made it more likely that the Rock-binding site was formed by both SD2 chains. Given the large and extended dimerization interface, we were concerned that small perturbations, such as single–amino acid changes, might not destabilize enough of the Shrm–Shrm interface to result in measurable changes in either dimerization or Rock binding. To avoid this potential problem, we used sequence conservation combined with our structural data to identify regions where alterations within the Shrm–Shrm interface may have the greatest impact. We identified two regions and generated multiple substitutions to target these regions (Figure 3A and Supplemental Figure S1). We termed these variants homodimerization (HD) mutants. One interface mutant, HD1 (^{1468}LLSL^{1471} to AASA; Figure 3A), primarily targets the body segment, whereas the second HD mutant, HD2 (^{1546}LIADARDL^{1553} to AAADARDA; Figure 3A), primarily targets the coiled-coil within the arm segment. These amino acid changes are also predicted to weaken contacts between the arm and body segments but to a lesser degree. The selected amino acids were changed to alanine, as its high helical propensity should minimize effects due to alterations in secondary structure. We expressed and purified these proteins and compared their elution profile in gel filtration to wild-type protein (Figure 3B). We observe distinct changes with both mutants; protein containing the HD1 substitution elutes in a single broad peak distinct from both species observed with the wild-type protein. HD2 has an equally pronounced but different effect, in which much of the dimeric peak has been shifted into a larger, uncharacterized species. We isolated protein corresponding to dimer in the case of HD2 or to the majority peak from HD1 purification (Figure 3B) and further characterized the effect of substitutions within the dimerization interface. We first tested their ability to form homodimers in solution by chemical cross-linking (Figure 3C). In this assay, both HD mutants exhibited reduced cross-linking when compared with wild type, indicating a change in the dimeric interface. It should be noted that the substitutions in HD1 are more severe and perturb dimerization to a greater extent than those substitutions in HD2. To further confirm that our HD variants perturb the structure of SD2, we probed their stability via limited proteolysis using the nonspecific enzyme subtilisin A (Supplemental Figure S3). Although still readily expressed and purified, both HD variants are more accessible to protease, indicating a disruption of the dimerization interface. Consistent with the data obtained in the cross-linking experiment described here, HD1 appears to be more sensitive to proteolysis. We then tested the ability of the HD mutant proteins to bind dRock by native gel electrophoresis (Figure 3D). Neither variant is able to bind the dRock-SBD (724–938), indicating that these substitutions alter the positions of residues within Shrm that are required for Rock

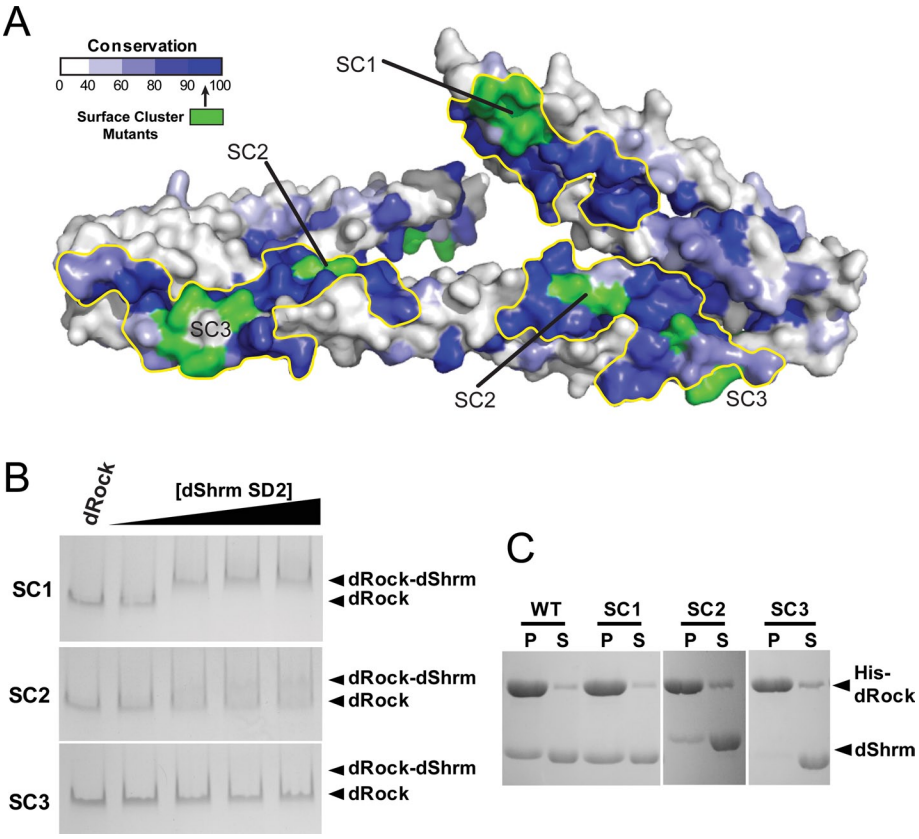

FIGURE 4: Conserved surfaces on SD2 are important for dRock binding. (A) Surface of SD2 with sequence conservation mapped in shades of blue. Invariant residues within SC mutants are shown in green. Three extended surfaces with high sequence conservation are outlined in yellow for clarity. (B) Native gel electrophoresis of dRock mixed with the indicated SD2 mutants. (C) Pull-down assay using His-dRock and indicated SD2 mutants.

binding. Taken together, these data indicate that mutations that perturb the Shrm–Shrm interface have a dramatic effect on Rock binding and suggest that the Rock-binding site on Shrm is composed of elements from both chains of the dimer.

A conserved Rock-binding interface on the SD2 surface

On the basis of the forgoing results, we hypothesized that we would be able to identify patches of surface residues that are required for binding to Rock but are not involved in dimerization. To test this, we searched for conserved patches of amino acids on the surface on the SD2 dimer by aligning 12 Shrm sequences from both vertebrate and invertebrate organisms (Supplemental Figure S1). We then used the RISLER matrix (Risler *et al.*, 1988), as implemented in ESPRIPT (Gouet *et al.*, 1999), to score and map conservation onto the SD2 surface (Figure 4A). Although this domain is highly conserved throughout its entire sequence, we identified three clusters of highly conserved residues as candidates for the Rock-binding surface. Two of these surfaces lie on opposite faces of the main body segment within helix B, whereas a third surface is formed by residues within helix A found near the end of the arm segment (Figure 4A). It should be noted that these patches are derived from amino acids residues on both the A and B chains, supporting the hypothesis that dimerization may be required to form a functional binding surface.

To address the importance of these surface clusters in Rock binding, we used the structural data to design amino acid substitutions within these potentially important surfaces. Given the preponderance of invariant residues, their broad distribution, and the elongated nature of the conserved clusters, we were concerned that the in vitro binding studies may not prove sensitive enough to observe changes resulting from single–amino acid changes. Therefore we designed three multiresidue variants with alterations on the SD2 surface while avoiding residues that could play a role in dimerization. The surface cluster (SC) variants are ^{1402}KMDEL^{1406} to AMDRA, ^{1470}SLSERLA^{1476} to ALEEDLE, and ^{1509}LKSDIERR^{1516} to AASDIEDA, which for clarity are named SC1, SC2, and SC3, respectively. The locations of these substitutions within the SD2 surface are indicated in Figure 4 (green residues). The elution profiles for the surface cluster variants were largely unchanged relative to wild type, suggesting that these mutations do not significantly alter the overall structure of the SD2 dimer (Supplemental Figure S5). We tested the surface cluster variants for their ability to bind dRock-SBD by pull-down (Figure 4C). In this assay, His-tagged dRock effectively precipitates wild-type SD2 and SC1. In contrast, this interaction is abrogated by substitutions made in SC2 and 3. We also monitored formation of a dShrm–dRock complex by native gel electrophoresis (Figure 4B). Similar to the results with the pull-down, SC1 binds dRock-like wild type, whereas complex formation with SC3 is undetectable. Although we could detect some complex formation with the SC2 variant, binding is clearly reduced, indicating that the targeted amino acids are located within the Rock-binding surface. These data indicate that Rock binding is most likely mediated by amino acids within the body segment, whereas the cluster of conserved residues within the arm is not involved. This supports the hypothesis that the Rock-binding site is composed of residues on the surface of the SD2 dimer. Further, since the SC2 derivative exhibits an intermediate level of binding, we conclude that these amino acids may lie at the periphery of the Rock binding site, whereas SC3 contains residues that are more critical for Rock binding.

The Rock-binding interface is conserved in vertebrate Shroom

We next tested whether the residues we show play an important role in Shrm–Rock binding in *Drosophila* are conserved in vertebrates. We noted that there was considerable sequence conservation within SD2s from various vertebrate Shrm proteins, so we chose to examine the effect of mutations within the context of mouse Shrm3 due to its ability to induce apical constriction in MDCK cells. The following amino acid changes were made in mShrm3 SD2 and the subsequent proteins tested for the ability to homodimerize and bind to the SBD of human Rock1: ^{1766}KKAEL^{1770} to AKARA (SC1), ^{1834}SLSGRLA^{1840} to ALEADLE (SC2), ^{1878}LKENLDRR^{1885} to AAENLDDA (SC3), ^{1832}LLSL^{1835} to AASA (HD1), and ^{1915}LLIEQRKL^{1922} to ALIEQAKA (HD2). All of the homodimerization and surface cluster mutations were generated in a plasmid encoding glutathione *S*-transferase (GST)–tagged mShrm3 SD2. Purified proteins were first tested for the ability to bind the hRock SBD (Figure 5A). In this

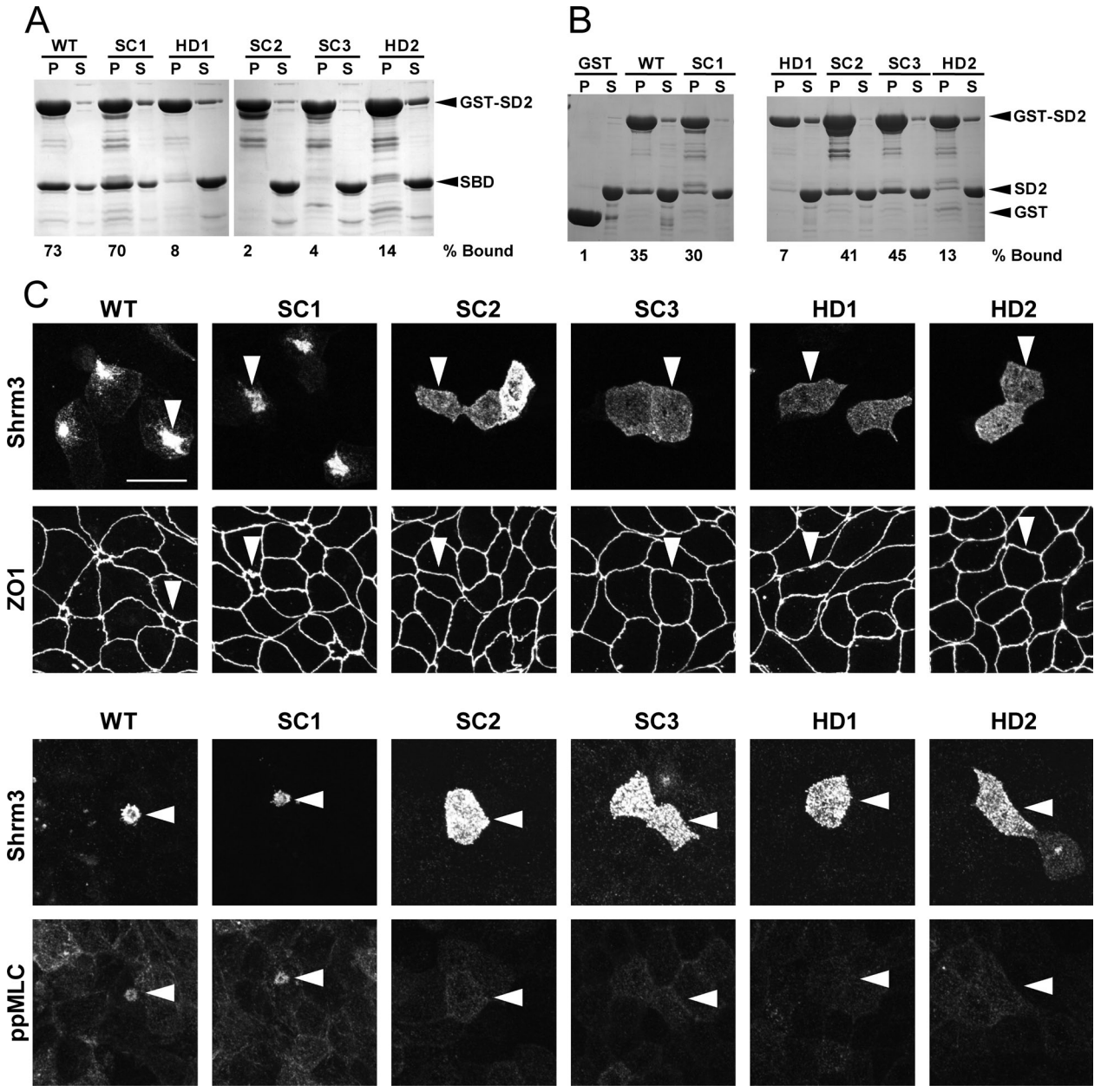

FIGURE 5: The Rock-binding interface is conserved in vertebrate Shroom. (A) Wild-type and mutant GST-tagged mouse Shrm3 SD2 proteins were mixed with untagged hRock as indicated and complexes detected by pull-down with glutathione resin followed by SDS–PAGE and Coomassie staining. (B) The ability of GST-tagged interface or surface cluster mutants to bind untagged mShrm3 SD2 was tested by a pull-down assay. (C) Wild-type and SD2 mutant versions of endolyn-tagged mShrm3 were expressed in MDCK cells and cells stained to detect Shrm3, ZO-1, and ppMLC. Only the wild type and the SD1 variant induce apical constriction and recruitment of active myosin II when targeted to the apical membrane. Transfected cells are denoted by arrowheads; scale bar, 20 μm.

assay, we could not detect binding of either of the homodimerization variants to the Rock SBD. For the surface cluster derivatives, binding of variant 1 to Rock was unaltered, whereas surface cluster variants 2 and 3 were incapable of binding Rock. These results are consistent with those obtained using the *Drosophila* proteins but suggest that the surface cluster 2 region of mouse Shrm3 may play a more significant role in binding to Rock. We next assayed the ability of the surface cluster and homodimerization variants to form homodimers with an untagged, wild-type mShrm3-SD2 (Figure 5B). As expected from our studies with dShrm, the homodimerization mutations severely impaired dimerization, whereas the surface cluster mutations had no effect on binding to SD2. It should be noted that the surface cluster variant 1 bound with slightly reduced efficiency. On the basis of these data, we conclude that the Rock-binding interface identified in *Drosophila* is largely conserved in the mouse proteins and that this Shrm–Rock binding module has been conserved across animal evolution at both the molecular and functional levels.

The Rock-binding surface is required for apical constriction

Our previous work showed that the SD2 motif of Shrm3 is both necessary and sufficient to cause apical constriction of polarized

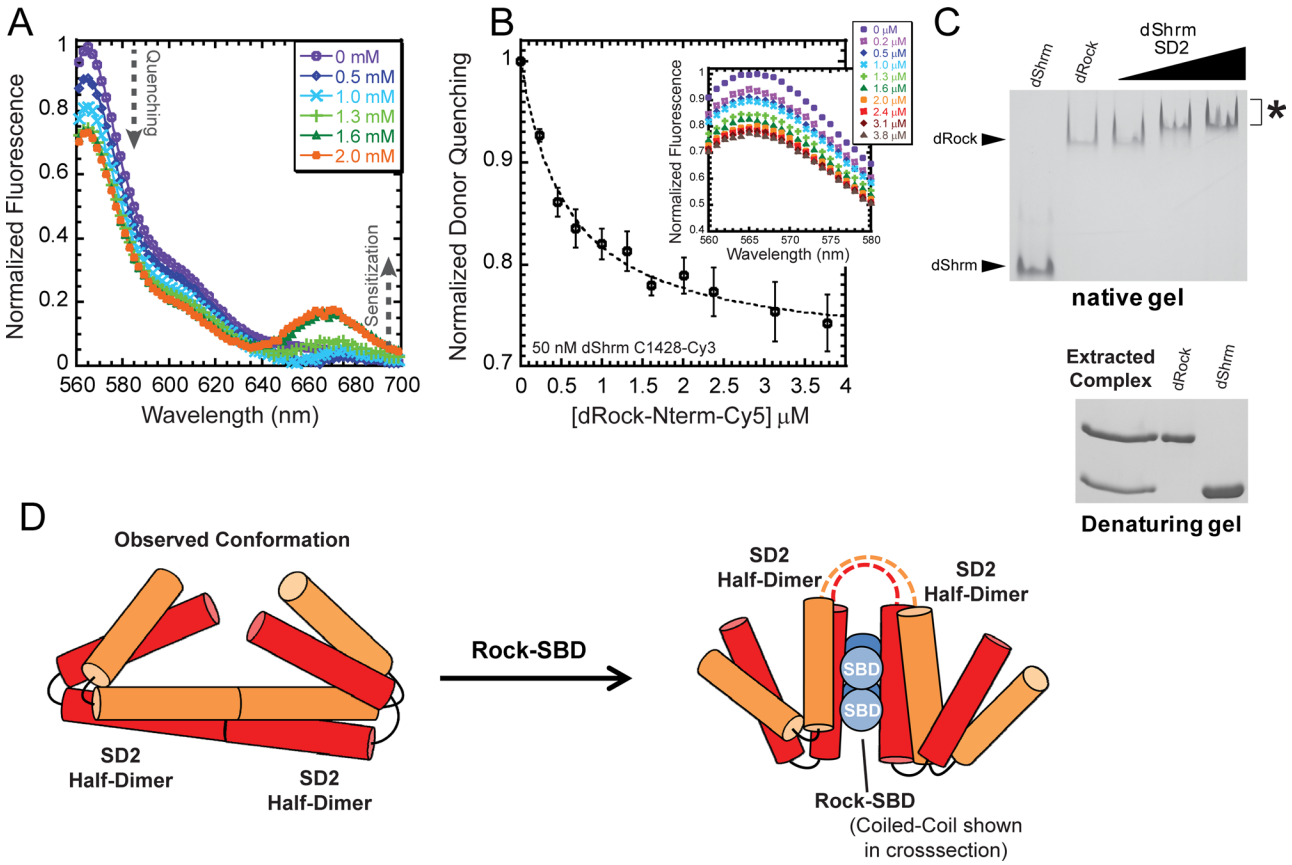

FIGURE 6: Characterizing the Shrm–Rock complex. (A) FRET titration of Cy5-labeled dRock into 50 nM Cy3-labeled dShrm showing donor quenching and acceptor sensitization for representative concentrations. (B) Donor quenching plotted as a function of Rock concentration and fitted to a single-binding mode to give a K_d value of 0.58 ± 0.07 μM. The error bars show the SE for the average of at least three independent experiments. (C) Estimation of the Shrm–Rock complex stoichiometry. Native-PAGE stained with colloidal blue was used to identify the Shrm–Rock complex as described earlier. Bands corresponding to the complex (denoted by the asterisk) were excised from native-PAGE, protein eluted from the gel slice, and run on SDS–PAGE to separate the components contained within. (D) Models describing one potential mode of interaction between Shrm SD2 and Rock formed by hinging at the symmetry point within the observed SD2 dimer.

epithelial cells when targeted to the apical domain of the cell (Hildebrand, 2005). To test whether alterations to the dimerization interface or the Rock-binding surface affect the ability of the Shrm3 SD2 to induce apical constriction, we introduced our homodimerization and surface cluster amino acid substitutions into the endolyn–mShrm3 chimeric protein. All of the endolyn–Shrm3 variants are expressed at equal levels and are efficiently targeted to the apical surface (Figure 5C, arrowheads). Consistent with the in vitro binding results, we observed that only the wild type and the surface cluster 1 variant retained the capacity to trigger apical constriction in cells.

To determine whether the various homodimerization and surface cluster mutants were capable of activating the Rock–myosin II pathway, we stained cells expressing each of the SD2 mutants to detect the myosin light chain (MLC) phosphorylated at Thr-18 and Ser-19 (ppMLC), a readout of active myosin II. Consistent with the in vitro binding assay and the foregoing results, only wild type and the surface cluster variant 1 of endolyn–Shrm3 showed recruitment of activated myosin II to the constricted apical surface (Figure 5C). By measuring the increase in apical fluorescence relative to the decrease in apical area, we estimate that there was an approximate 1.4- to 1.8-fold increase in the amount of apically localized active myosin II. In contrast, neither homodimerization variant nor the surface cluster variants 2 or 3 caused apical constriction, and there was no enrichment of active myosin II. These data suggest that in vivo, the SD2 motif must retain the ability to both dimerize and bind Rock in order to trigger apical constriction and that Shrm3-mediated apical contraction is dependent on the activity of both Rock and myosin.

Characterizing the Shrm–Rock complex

In an effort to elucidate the molecular details of the Shrm–Rock complex, we first used fluorescence energy transfer (FRET) experiments to detect and quantify the interaction between dShrm and dRock SBD. Because the precise binding interface between dRock and dShrm is unknown, we labeled dRock with Cy5 at its N-terminus, whereas dShrm SD2 was labeled with Cy3 at a single cysteine (C1428) not believed to be located within the Rock-binding interface. There are two endogenous cysteines within this fragment of dShrm, so a conservative mutant of dShrm (C1533S) was generated for this assay to ensure labeling at a single position. Titration of dShrm with dRock resulted in a decrease in donor emission and increase in acceptor emission consistent with an increase in FRET due to a binding interaction (Figure 6A). Assuming a single-binding mode for this interaction, we calculate the equilibrium K_d to be 0.58 ± 0.07 μM (Figure 6B). This affinity is comparable to that of RhoA, which has a reported K_d of 0.13 μM (Blumenstein and Ahmadian, 2004).

We next examined the stoichiometry of the dShrm–dRock complex. To determine this, we mixed purified dRock SBD and dShrm SD2 in solution to form a complex and then resolved it on a native gel. After electrophoresis, the complexes were excised from the gel, eluted, resolved by SDS–PAGE, and detected by Coomassie blue staining (Figure 6C). Alternatively, complex was run on a gel filtration column and peak fractions were resolved by SDS–PAGE. The ratio of SD2 to SBD in the complex was measured by densitometry and corrected for the relative molecular masses of the two proteins (Supplemental Figure S4). In all cases, isolated complexes were composed of SD2 and SBD in an ~1:1 molar ratio. Although the possibility for a variety of higher-order species cannot be ruled out from these data, we feel that heterodimeric and heterotetrameric species are the most probable. This is consistent with RhoA, which also interacts with Rock in a 1:1 molar ratio, and places important mechanistic constraints on the complex.

DISCUSSION

Shroom domain 2 adopts a unique fold

Our studies of SD2 reveal that this motif is composed of an unusual arrangement of three canonical coiled-coil segments. On the basis of the structure and in vitro binding assays, we propose that two binding surfaces within SD2 are important for Rock interaction. The first mediates SD2 dimerization, which in turn positions conserved residues on the SD2 surface into an orientation that is competent for Rock binding. Conserved residues on the surface are located in three clusters; however, only residues within the main body were shown to play a role in Rock binding. The conserved patches within the main body segment contain residues from both molecules of the SD2 dimer, which may explain why dimerization is required for Rock binding. The observed symmetry within the SD2 dimer dictates that there are two independent but identical Rock-binding sites. Of importance, any mutation that disrupts Rock binding also abrogates Shrm-induced apical constriction in vivo.

The Shrm–Rock complex

Crystal structures of the coiled-coil portion of Rock indicate that it exists as a dimer (Shimizu *et al.*, 2003; Dvorsky *et al.*, 2004; Tu *et al.*, 2011), and our data suggest that the Shrm–Rock complex contains equal ratios of SD2 and SBD. Of the possible stoichiometries for the Shrm–Rock complex, we speculate that heterodimeric or heterotetrameric (a dimer of dimers) species are most probable, and we favor the latter for the following reasons. First, both Shrm and Rock components are dimers in solution. Second, a Shrm–Rock heterodimer would require that both the SD2 and SBD homodimers separate before reforming the heterodimer. We predict that there would be a large energetic barrier to this rearrangement. Third, our results indicate that distinct surfaces are required for Rock binding and SD2 homodimerization. Finally, the crystal structure of the Rock–RhoA complex indicates that dimerization of the Rho-binding domain is not altered upon binding to RhoA (Dvorsky *et al.*, 2004).

Molecular models for the Shrm–Rock complex

The dShrm SD2 structure presented here places a number of constraints on how it interacts with the SBD of Rock. Previous studies showed that regions of Rock just N-terminal and C-terminal of the Shrm-binding domain form a parallel coiled-coil dimer (Dvorsky *et al.*, 2004; Tu *et al.*, 2011). On the basis of these studies, it is reasonable to predict that Rock's Shrm-binding domain also exists as a parallel coiled-coil. If this is the case, we can envision two different models for the Shrm–Rock interaction based on our structures. In the first model, it is possible that the Shrm SD2 dimer binds the SBD dimer without a major disruption to the observed SD2 conformation. We do not favor this model, however, because it is difficult to envision how the two Rock-binding interfaces, one in each half-dimer, would contact the two independent Shrm-binding sites that would be generated by the nature of the parallel coiled-coil of the Shrm-binding domain. Instead we favor a model in which there is a large conformational change upon Rock binding that allows the SD2 to position its half-dimers on opposite sides of the Rock coiled-coil (Figure 6D). This would allow the two surface clusters that bind to Rock to interact with the helices of the SBD simultaneously. A direct observation of SD2 in other conformations or bound to Rock will be required to address this.

Implications of the Shroom–Rock interaction

It has been shown that Shrm–Rock interactions are vital for several developmental processes, including neural tube, lens, and gut morphogenesis. There is no information about the stoichiometry or affinity of the complex, and it is unclear how the Shrm–Rock interaction may by regulated. There are two primary models for thinking about how Shrm may function with Rock to achieve localized activation of contractile actomyosin networks. First, Shrm binding to Rock leads to both the redistribution of Rock and the activation of its catalytic activity. Second, it is possible that Shrm binding can alter the distribution of Rock but that additional inputs activate Rock. Our results indicate that Shrm and Rock bind with high affinity and are likely to form a heterotetramer in solution. On the basis of the fact that Shrm binds to Rock in close proximity to the Rho-binding site, it is tempting to speculate that Shrm binding activates Rock in a manner similar to Rho. However, additional structural studies and kinetic assays will be required to verify this hypothesis.

Genetic and cell-based approaches demonstrated that the Rock–myosin II pathway is used to control the cell behaviors that facilitate tissue morphogenesis in animals. As a result, targeted Rock inhibition is viewed as a viable therapeutic approach for treating many clinical conditions, including cancer (Liu *et al.*, 2011), obesity (Hara *et al.*, 2011), type I diabetes (Biswas *et al.*, 2011), pulmonary hypertension (Connolly and Aaronson, 2011), and many others (reviewed in Dong *et al.*, 2011). The central role of Rock also makes global inhibition of Rock a challenge due to possible side effects. Therefore it would be of great benefit to be able to target specific steps of Rock activation or specific effectors of Rock. One of the ways to accomplish this is to understand how specific proteins interact with Rock and elucidate the outcomes of these interactions on Rock activity. The identification of the Shrm–Rock interaction as a distinct module that may function independent of RhoA may provide ways to abrogate or enhance specific arms of Rock signaling while leaving others unperturbed.

MATERIALS AND METHODS

Protein expression and purification

Coding sequences for dShrm SD2 (residues 1393–1576) and dRock SBD (724–938) were amplified by PCR and cloned into the bacterial expression vector pET151-D/Topo (Invitrogen, Carlsbad, CA). Protein expression was performed in BL21(DE3) *Escherichia coli* cells using ZY autoinduction media (Studier, 2005) at room temperature for ~24 h, harvested by centrifugation, and lysed via homogenization in 25 mM Tris, pH 8.0, 500 mM NaCl, 10% glycerol, 5 mM imidazole, and 5 mM β-mercaptoethanol. The lysate was cleared by centrifugation at 100,000 × *g*. dSD2 was purified by nickel affinity chromatography (Qiagen, Valencia, CA), followed by overnight digestion with tobacco etch virus (TEV) protease. A second round of nickel affinity purification was performed to remove the liberated

His tag, TEV protease, and many nonspecific contaminants. Gel filtration, using a Sephacryl S-200 gel filtration column (GE Healthcare, Piscataway, NJ), was performed, and peak fractions were concentrated to 9 mg/ml in 20 mM Tris, pH 8.0, 0.5 M NaCl, 8% glycerol, and 5 mM dithiothreitol (DTT) using a Vivaspin concentrator (Millipore, Billerica, CA) before crystallization. The purity was typically >99% as verified by SDS–PAGE. Selenomethionine-substituted dShrm SD2 was expressed using PASM media (Studier, 2005), and purification was essentially the same as for the native protein. Purification of dRock SBD (724–938) was aided by the addition of an anion exchange chromatography step before gel filtration.

Mutant mShrm3 and dShrm SD2 proteins

SC and HD mutations in mShrm3 and dShrm were made using the QuikChange Site-Directed Mutagenesis Kit (Stratagene, Santa Clara, CA). The mutant dShrm SD2 proteins were expressed and purified in a manner similar to the wild type. All biochemical assays with wild-type and HD proteins were performed with the indicated protein fractions from gel filtration (Figure 3B). Gel filtration profiles for Shrm SD2 proteins containing the SC1, SC2, or SC3 substitution were are highly similar to that of wild-type SD2, with the exception of some nucleic acid contamination in the SC1 and SC2 purifications. This was separated by gel filtration, and fractions corresponding to the crystallized peak were used for all biochemical assays (Supplementary Figure S5). For mShrm3 mutants, mutagenesis was performed on mShrm3 in the pCS2-endolyn-Shrm3 expression plasmid. For in vitro expression of mShrm3 SD2 mutant proteins, the mutated sequence encoding amino acids 1562–1986 was cloned from the endolyn–Shrm3 vectors in pGex-2TK for expression in *E. coli* CodonPlus (RIPL) cells. Recombinant proteins were expressed and purified as described (Farber *et al.*, 2011).

Crystallization of *Drosophila* Shroom SD2

Single thick, rod-shaped crystals were obtained for dShrm SD2 via the vapor diffusion method with a reservoir solution containing 0.1 M 2-(*N*-morpholino)ethanesulfonic acid (MES) at pH 6.0, 1.35 M K/Na tartrate, 0.7 M sodium thiocyanate, 11% glycerol (vol/vol), and 4 mM DTT. Crystals grew at 4°C in 7–10 d with a typical size of $80 \times 40 \times 500$ μm and were cryoprotected by transition of the crystal into a buffer containing 0.1 M MES, 1.4 M K/Na tartrate, 0.9 M sodium thiocynate, 15% glycerol, and 4 mM DTT. The cryoprotected crystals were flash frozen under liquid nitrogen before data collection. The same procedure was used to crystallize and cryoprotect SeMET-substituted SD2.

Structure determination

SD2 crystals belong to space group $P2_12_12$, with a = 72.6 Å, b = 85.6 Å, and c = 93.0 Å. Diffraction data from both native and SeMET dShrm SD2 crystals were collected at beamline X25 at the National Synchrotron Light Source, Brookhaven National Laboratory. Diffraction data integration, scaling, and merging were performed using HKL2000 (Otwinowski and Minor, 1997). Initial phases were estimated via the SAD method using SHELX C/D/E (Sheldrick, 2008), which found six of the possible eight selenium sites. An initial model was built into these experimental maps using Coot (Emsley and Cowtan, 2004). This model was then further refined against native data and the model improved using a combination of simulated annealing and positional, B factor, and TLS refinement (Zucker *et al.*, 2010) within Phenix (Adams *et al.*, 2010). Model quality was monitored using MolProbity (Davis *et al.*, 2007). All structural images in this article were generated using PyMOL (www.pymol.org). The coordinates and structure factors for the *Drosophila* SD2 structure presented in this article have been submitted to the Protein Data Bank (www.rcsb.org/pdb/home/home.do) and assigned the identifier 3THF.

Chemical cross-linking

dShrm SD2 was incubated with the indicated concentration of glutaraldehyde in a reaction buffer containing 25 mM 4-(2-hydroxyethyl)-1-piperazineethanesulfonic acid (HEPES), pH 7.5, 8% glycerol, 500 mM NaCl, and 5 mM β-mercaptoethanol, with a final dShrm SD2 concentration of 8 μM. At each time point, 20 μl of the cross-linking reaction was removed and the reaction stopped with 2 μl of 1.0 M Tris at pH 8.0 and the sample subjected to SDS–PAGE and visualized using Coomassie blue staining.

Complex formation

Equal molar quantities of dShrm SD2 and dRock SBD were mixed at a combined concentration of 2.4 mg/ml and dialyzed into 25 mM Tris, pH 8.0, 8% glycerol, 150 mM NaCl, and 5 mM β-mercaptoethanol. Complex was isolated using a Sephacryl S-300 gel filtration column (GE Healthcare). The SD2–SBD complex eluted off the gel filtration column in one peak distinct from that for SD2 or SBD alone. For solution binding and native gel electrophoresis, a fixed concentration (5 μM) of dRock 724–938 was mixed with increasing concentration of dShrmSD2 (1–10 μM) and incubated for 1 h. Samples were then loaded on 8% PAGE gels and resolved by electrophoresis at 4°C. Proteins were detected with Coomassie blue. For GST pull-down assays using mShrm3, either wild-type GST-Shrm3 SD2 or SC and HD mutant versions (spanning amino acids 1562–1986) bound to beads were mixed with soluble, untagged mShrm3 SD2 (residues 1762–1952) or hRock1 (residues 707–946). Complexes were washed with NETN (100 mM NaCl, 1 mM EDTA, 20 mM Tris, pH 8.0, 0.05% NP-40), resuspended in SDS–PAGE sample buffer, resolved by SDS–PAGE, and detected using Coomassie blue.

Apical constriction assays

MDCK cells were grown in EMEM supplemented with 10% fetal bovine serum, penicillin/streptavidin, and L-glutamine. Apical constriction assays using endolyn–dShrm, endolyn–Shrm3, endolyn–mShrm3 dlSD2, or endolyn–Shrm3 harboring SC or HD were performed and imaged as described (Hildebrand, 2005). Cells were attained with the following antibodies: UPT132 (1:250, rabbit anti-Shrm3; Hildebrand, 2005), rat anti-ZO1 (1:500; Chemicon, Temecula, CA), and rabbit anti–pThr18/pSer19 MLC2 (1:50; Cell Signaling Technology, Beverly, MA). Primary antibodies were detected using Alexa 488 or 568–conjugated secondary antibodies (1:400; Invitrogen). Images were acquired using a Bio-Rad Radiance 2000 Laser Scanning System (Bio-Rad, Hercules, CA) mounted on a Nikon E800 microscope (Nikon, Melville, NY) with 40× and 60× oil objectives and processed using either ImageJ (National Institutes of Health, Bethesda, MD) or Photoshop (Adobe, San Jose, CA). The fluorescence intensity of ppMLC was determined using ImageJ and was achieved by measuring the average fluorescence intensity of a fixed region of interest (ROI) at the apical surface of subsaturated confocal images from expressing and nonexpressing cells. Fluorescence intensity of the ROI was then corrected for the decrease in area of apically constricted cells ($n \leq 20$ cells/variant). Change in fluorescence intensity was then determined as the ratio of the corrected intensity of constricted versus nonconstricted cells.

Fluorescence labeling

dShrm was labeled at the N-terminus with Alexa 594 succinimidyl ester (Invitrogen) in amino labeling buffer (20 mM HEPES, pH 7.0, 100 mM NaCl, 8% glycerol) or at C1428 of the C1533S mutant with

Cy3 or Cy5 maleimide (GE Healthcare) in cysteine labeling buffer (20 mM HEPES, pH 7.6, 100 mM NaCl, 8% glycerol). Small (821–938) dRock was labeled at C862 with Cy3 maleimide as described. Large dRock (724–938) was labeled at the N-terminus with Cy5 succinimidyl ester (GE Healthcare) in amino labeling buffer. All labeling reactions included 10× molar excess of fluorophore at room temperature for 2 h. Excess fluorophore was removed from the samples through extensive dialysis with labeling buffer. The labeling efficiency was quantified using the extinction coefficient of the dye compared with the protein concentration determined from a standard curve using a Bradford assay and found to be essentially 1:1.

FRET binding experiments

FRET titrations were performed in dShrm reaction buffer, using a 50 nM of Cy3-labeled dShrm or dRock and increasing concentrations of Cy5-labeled dRock or dShrm. Cy3 was excited at 552 nM, and the donor emission maximum (563 nm) was corrected for dilution, normalized, and plotted as a function of protein concentration as the average of three independent experiments. Fluorescence quenching (F_Q) titrations were fitted to a single binding equation:

$$F_Q = \frac{\Delta F_Q \times [\text{dRock}]}{K_d + [\text{dRock}]}$$

where ΔF_Q is the normalized change in donor fluorescence intensity and K_d is the dissociation constant.

ACKNOWLEDGMENTS

We thank Jeff Brodsky and Karen Arndt for critical comments on the manuscript. Operations at the National Synchrotron Light Source are supported by the Department of Energy, Office of Basic Energy Research, and by the National Institutes of Health. Data collection at the National Synchrotron Light Source was funded by the National Center for Research Resources. This work was supported by National Institutes of Health Grant GM097204.

REFERENCES

Adams PD *et al.* (2010). PHENIX: a comprehensive Python-based system for macromolecular structure solution. Acta Crystallogr D Biol Crystallogr 66, 213–221.

Amano M, Chihara K, Nakamura N, Kaneko T, Matsuura Y, Kaibuchi K (1999). The COOH terminus of Rho-kinase negatively regulates Rho-kinase activity. J Biol Chem 274, 32418–32424.

Amano M, Ito M, Kimura K, Fukata Y, Chihara K, Nakano T, Matsuura Y, Kaibuchi K (1996a). Phosphorylation and activation of myosin by Rho-associated kinase (Rho-kinase). J Biol Chem 271, 20246–20249.

Amano M, Mukai H, Ono Y, Chihara K, Matsui T, Hamajima Y, Okawa K, Iwamatsu A, Kaibuchi K (1996b). Identification of a putative target for Rho as the serine-threonine kinase protein kinase N. Science 271, 648–650.

Biswas PS, Gupta S, Chang E, Bhagat G, Pernis AB (2011). Aberrant ROCK activation promotes the development of type I diabetes in NOD mice. Cell Immunol 266, 111–115.

Blumenstein L, Ahmadian MR (2004). Models of the cooperative mechanism for Rho effector recognition: implications for RhoA-mediated effector activation. J Biol Chem 279, 53419–53426.

Bolinger C, Zasadil L, Rizaldy R, Hildebrand J (2010). Specific isoforms of *Drosophila* Shroom define spatial requirements for the induction of apical constriction. Dev Dyn 239, 2078–2093.

Chung MI, Nascone-Yoder NM, Grover SA, Drysdale TA, Wallingford JB (2010). Direct activation of Shroom3 transcription by Pitx proteins drives epithelial morphogenesis in the developing gut. Development 137, 1339–1349.

Connolly MJ, Aaronson PI (2011). Key role of the RhoA/Rho kinase system in pulmonary hypertension. Pulm Pharmacol Ther 24, 1–14.

Davis IW *et al.* (2007). MolProbity: all-atom contacts and structure validation for proteins and nucleic acids. Nucleic Acids Res 35, W375–W383.

Dietz ML, Bernaciak TM, Vendetti F, Kielec JM, Hildebrand JD (2006). Differential actin-dependent localization modulates the evolutionarily conserved activity of Shroom family proteins. J Biol Chem 281, 20542–20554.

Dong M, Yan BP, Liao JK, Lam YY, Yip GW, Yu CM (2011). Rho-kinase inhibition: a novel therapeutic target for the treatment of cardiovascular diseases. Drug Discov Today 15, 622–629.

Dvorsky R, Blumenstein L, Vetter IR, Ahmadian MR (2004). Structural insights into the interaction of ROCKI with the switch regions of RhoA. J Biol Chem 279, 7098–7104.

Emsley P, Cowtan K (2004). Coot: model-building tools for molecular graphics. Acta Crystallogr D Biol Crystallogr 60, 2126–2132.

Fairbank PD, Lee C, Ellis A, Hildebrand JD, Gross JM, Wallingford JB (2006). Shroom2 (APXL) regulates melanosome biogenesis and localization in the retinal pigment epithelium. Development 133, 4109–4118.

Farber MJ, Rizaldy R, Hildebrand JD (2011). Shroom2 regulates contractility to control endothelial morphogenesis. Mol Biol Cell 22, 795–805.

Gouet P, Courcelle E, Stuart DI, Metoz F (1999). ESPript: analysis of multiple sequence alignments in PostScript. Bioinformatics 15, 305–308.

Hagens O, Ballabio A, Kalscheuer V, Kraehenbuhl JP, Schiaffino MV, Smith P, Staub O, Hildebrand J, Wallingford JB (2006a). A new standard nomenclature for proteins related to Apx and Shroom. BMC Cell Biol 7, 18.

Hagens O *et al.* (2006b). Disruptions of the novel KIAA1202 gene are associated with X-linked mental retardation. Hum Genet 118, 578–590.

Haigo SL, Hildebrand JD, Harland RM, Wallingford JB (2003). Shroom induces apical constriction and is required for hingepoint formation during neural tube closure. Curr Biol 13, 2125–2137.

Hara Y *et al.* (2011). Rho and Rho-kinase activity in adipocytes contributes to a vicious cycle in obesity that may involve mechanical stretch. Sci Signal 4, ra3.

Hildebrand JD (2005). Shroom regulates epithelial cell shape via the apical positioning of an actomyosin network. J Cell Sci 118, 5191–5203.

Hildebrand JD, Soriano P (1999). Shroom, a PDZ domain-containing actin-binding protein, is required for neural tube morphogenesis in mice. Cell 99, 485–497.

Ikebe M, Koretz J, Hartshorne DJ (1988). Effects of phosphorylation of light chain residues threonine 18 and serine 19 on the properties and conformation of smooth muscle myosin. J Biol Chem 263, 6432–6437.

Ishizaki T *et al.* (1996). The small GTP-binding protein Rho binds to and activates a 160 kDa Ser/Thr protein kinase homologous to myotonic dystrophy kinase. EMBO J 15, 1885–1893.

Jacobs M, Hayakawa K, Swenson L, Bellon S, Fleming M, Taslimi P, Doran J (2006). The structure of dimeric ROCK I reveals the mechanism for ligand selectivity. J Biol Chem 281, 260–268.

Kawano Y, Fukata Y, Oshiro N, Amano M, Nakamura T, Ito M, Matsumura F, Inagaki M, Kaibuchi K (1999). Phosphorylation of myosin-binding subunit (MBS) of myosin phosphatase by Rho-kinase in vivo. J Cell Biol 147, 1023–1038.

Kimura K *et al.* (1996). Regulation of myosin phosphatase by Rho and Rho-associated kinase (Rho-kinase). Science 273, 245–248.

Komander D, Garg R, Wan PT, Ridley AJ, Barford D (2008). Mechanism of multi-site phosphorylation from a ROCK-I:RhoE complex structure. EMBO J 27, 3175–3185.

Kottgen A *et al.* (2009). Multiple loci associated with indices of renal function and chronic kidney disease. Nat Genet 41, 712–717.

Lee C, Le MP, Wallingford JB (2009). The shroom family proteins play broad roles in the morphogenesis of thickened epithelial sheets. Dev Dyn 238, 1480–1491.

Liu X, Choy E, Hornicek FJ, Yang S, Yang C, Harmon D, Mankin H, Duan Z (2011). ROCK1 as a potential therapeutic target in osteosarcoma. J Orthop Res 29, 1259–1266.

Matsui T, Amano M, Yamamoto T, Chihara K, Nakafuku M, Ito M, Nakano T, Okawa K, Iwamatsu A, Kaibuchi K (1996). Rho-associated kinase, a novel serine/threonine kinase, as a putative target for small GTP binding protein Rho. EMBO J 15, 2208–2216.

Moussavi RS, Kelley CA, Adelstein RS (1993). Phosphorylation of vertebrate nonmuscle and smooth muscle myosin heavy chains and light chains. Mol Cell Biochem 127–128, 219–227.

Nishimura T, Takeichi M (2008). Shroom3-mediated recruitment of Rho kinases to the apical cell junctions regulates epithelial and neuroepithelial planar remodeling. Development 135, 1493–1502.

Otwinowski Z, Minor W (1997). Processing of x-ray diffraction data collected in oscillation mode. Methods Enzymol 276, 307–326.

Plageman TF Jr, Chung MI, Lou M, Smith AN, Hildebrand JD, Wallingford JB, Lang RA (2010). Pax6-dependent Shroom3 expression regulates apical

constriction during lens placode invagination. Development 137, 405–415.
Plageman TF Jr, Zacharias AL, Gage PJ, Lang RA (2011). Shroom3 and a Pitx2-N-cadherin pathway function cooperatively to generate asymmetric cell shape changes during gut morphogenesis. Dev Biol 357, 227–234.
Risler JL, Delorme MO, Delacroix H, Henaut A (1988). Amino acid substitutions in structurally related proteins. A pattern recognition approach. Determination of a new and efficient scoring matrix. J Mol Biol 204, 1019–1029.
Sheldrick GM (2008). A short history of SHELX. Acta Crystallogr A 64, 112–122.
Shimizu T, Ihara K, Maesaki R, Amano M, Kaibuchi K, Hakoshima T (2003). Parallel coiled-coil association of the RhoA-binding domain in Rho-kinase. J Biol Chem 278, 46046–46051.
Studier FW (2005). Protein production by auto-induction in high density shaking cultures. Protein Expr Purif 41, 207–234.
Taylor J, Chung KH, Figueroa C, Zurawski J, Dickson HM, Brace EJ, Avery AW, Turner DL, Vojtek AB (2008). The scaffold protein POSH regulates axon outgrowth. Mol Biol Cell 19, 5181–5192.
Trakselis MA, Alley SC, Ishmael FT (2005). Identification and mapping of protein-protein interactions by a combination of cross-linking, cleavage, and proteomics. Bioconjug Chem 16, 741–750.
Tu D, Li Y, Song HK, Toms AV, Gould CJ, Ficarro SB, Marto JA, Goode BL, Eck MJ (2011). Crystal structure of a coiled-coil domain from human ROCK I. PLoS One 6, e18080.
Wen W, Liu W, Yan J, Zhang M (2008). Structure basis and unconventional lipid membrane binding properties of the PH-C1 tandem of Rho kinases. J Biol Chem 283, 26263–26273.
Yamaguchi H, Kasa M, Amano M, Kaibuchi K, Hakoshima T (2006a). Molecular mechanism for the regulation of Rho-kinase by dimerization and its inhibition by fasudil. Structure 14, 589–600.
Yamaguchi H, Miwa Y, Kasa M, Kitano K, Amano M, Kaibuchi K, Hakoshima T (2006b). Structural basis for induced-fit binding of Rho-kinase to the inhibitor Y-27632. J Biochem 140, 305–311.
Zucker F, Champ PC, Merritt EA (2010). Validation of crystallographic models containing TLS or other descriptions of anisotropy. Acta Crystallogr D Biol Crystallogr 66, 889–900.